

Article

A Self-Assembling Amphiphilic Peptide Dendrimer-Based Drug Delivery System for Cancer Therapy

Dandan Zhu ^{1,†}, Huanle Zhang ^{1,†}, Yuanzheng Huang ¹, Baoping Lian ¹, Chi Ma ¹, Lili Han ¹, Yu Chen ¹, Shengmei Wu ², Ning Li ^{1,3,*} , Wenjie Zhang ¹ and Xiaoxuan Liu ^{1,*} 

- ¹ State Key Laboratory of Natural Medicines and Jiangsu Key Laboratory of Drug Discovery for Metabolic Diseases, Center of Advanced Pharmaceuticals and Biomaterials, China Pharmaceutical University, Nanjing 210009, China; 1831070168@stu.cpu.edu.cn (D.Z.); 1621010179@stu.cpu.edu.cn (H.Z.); 3120070206@stu.cpu.edu.cn (Y.H.); 3119070191@stu.cpu.edu.cn (B.L.); 1731070155@stu.cpu.edu.cn (C.M.); 1821070945@stu.cpu.edu.cn (L.H.); 1821070944@stu.cpu.edu.cn (Y.C.); wenjiezhang@cpu.edu.cn (W.Z.)
- ² Department of Analytical Chemistry, College of Science, China Pharmaceutical University, Nanjing 210009, China; 1020081878@cpu.edu.cn
- ³ School of Pharmacy, Fujian Medical University, Fuzhou 350122, China
- * Correspondence: ningli@fjmu.edu.cn (N.L.); xiaoxuanliu@cpu.edu.cn (X.L.)
- † These authors contributed equally to this work.



Citation: Zhu, D.; Zhang, H.; Huang, Y.; Lian, B.; Ma, C.; Han, L.; Chen, Y.; Wu, S.; Li, N.; Zhang, W.; et al. A Self-Assembling Amphiphilic Peptide Dendrimer-Based Drug Delivery System for Cancer Therapy. *Pharmaceutics* **2021**, *13*, 1092. <https://doi.org/10.3390/pharmaceutics13071092>

Academic Editors: Eduardo Ruiz-Hernandez, Amelia Ultimo, Luiza C. S. Erthal and Jaehwi Lee

Received: 19 June 2021

Accepted: 14 July 2021

Published: 17 July 2021

Publisher's Note: MDPI stays neutral with regard to jurisdictional claims in published maps and institutional affiliations.



Copyright: © 2021 by the authors. Licensee MDPI, Basel, Switzerland. This article is an open access article distributed under the terms and conditions of the Creative Commons Attribution (CC BY) license (<https://creativecommons.org/licenses/by/4.0/>).

Abstract: Despite being a mainstay of clinical cancer treatment, chemotherapy is limited by its severe side effects and inherent or acquired drug resistance. Nanotechnology-based drug-delivery systems are widely expected to bring new hope for cancer therapy. These systems exploit the ability of nanomaterials to accumulate and deliver anticancer drugs at the tumor site via the enhanced permeability and retention effect. Here, we established a novel drug-delivery nanosystem based on amphiphilic peptide dendrimers (AmPDs) composed of a hydrophobic alkyl chain and a hydrophilic polylysine dendron with different generations (AmPD KK₂ and AmPD KK₂K₄). These AmPDs assembled into nanoassemblies for efficient encapsulation of the anti-cancer drug doxorubicin (DOX). The AmPDs/DOX nanoformulations improved the intracellular uptake and accumulation of DOX in drug-resistant breast cancer cells and increased permeation in 3D multicellular tumor spheroids in comparison with free DOX. Thus, they exerted effective anticancer activity while circumventing drug resistance in 2D and 3D breast cancer models. Interestingly, AmPD KK₂ bearing a smaller peptide dendron encapsulated DOX to form more stable nanoparticles than AmPD KK₂K₄ bearing a larger peptide dendron, resulting in better cellular uptake, penetration, and anti-proliferative activity. This may be because AmPD KK₂ maintains a better balance between hydrophobicity and hydrophilicity to achieve optimal self-assembly, thereby facilitating more stable drug encapsulation and efficient drug release. Together, our study provides a promising perspective on the design of the safe and efficient cancer drug-delivery nanosystems based on the self-assembling amphiphilic peptide dendrimer.

Keywords: amphiphilic peptide dendrimer; self-assembling; drug delivery; cancer therapy

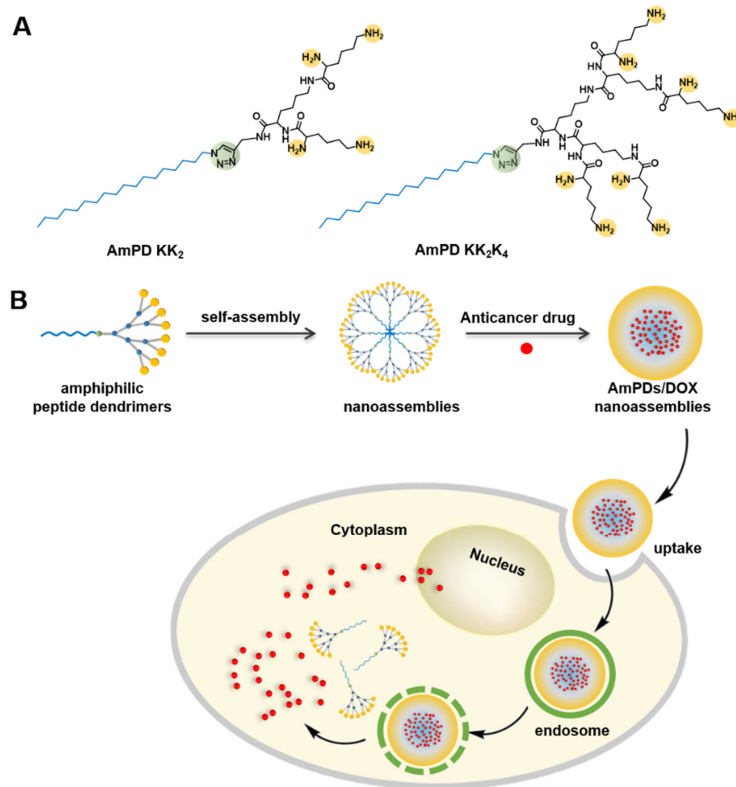
1. Introduction

Cancer is one of the leading causes of death around the world [1]. Although considerable achievements have been made in clinical cancer treatment, an effective cure remains a challenge [2]. The efficacy of chemotherapy—the mainstay of clinical cancer treatment—is limited by its severe side effects, which include high toxicity, poor tumor selectivity, and inherent or acquired drug resistance during or after chemotherapy [3–5]. To overcome the side effects of chemotherapy, numerous therapeutic strategies have been proposed. One particularly promising strategy is nanotechnology-based drug delivery systems (NDDSs) [6–9]. These NDDSs are able to facilitate the accumulation and delivery of anticancer drugs at tumor lesions via the enhanced permeability and retention (EPR) effect by virtue of their unique nanoscale size. This can significantly increase the local

concentration of the drugs and improve their therapeutic potency [10]. It is worth noting that the drug-loaded nanoparticles can be taken up by tumor cells via endocytosis, which can bypass drug efflux and increase the drug accumulation, hence overcoming drug resistance [11,12]. Therefore, the development of NDDSs brings new hope to revolutionize the therapeutic outcomes of cancer treatment.

Over the past decades, a variety of materials have been utilized to establish NDDSs for cancer therapy [7,13]. Among them, dendrimers—a special family of synthetic macromolecules furnished with a highly ramified architecture—have emerged as an attractive option because of their precisely defined structure and multivalent cooperativity [14,15]. In particular, amphiphilic dendrimers with judiciously tailored hydrophobic and hydrophilic components have been demonstrated to be able to self-assemble to supramolecular dendrimers for effective drug delivery in different disease models [16–20]. Recently, to combine the excellent properties of peptide dendrimers (such as their protein-like properties, good biocompatibility, etc. [21,22]), we developed amphiphilic peptide dendrimers (AmPDs), which carry peptide dendrons as hydrophilic heads for the delivery of nucleic acid therapeutics [23,24].

Herein, we exploit a novel NDDS based on AmPDs for the delivery of chemotherapeutics (Scheme 1). These AmPDs are composed of hydrophobic alkyl chain and hydrophilic polylysine dendron with different generations (AmPD KK₂ and AmPD KK₂K₄). Based on the amphiphilic nature, these AmPDs would self-assemble to form supramolecular dendrimer nanoassemblies with hydrophobic cavities that can encapsulate hydrophobic chemotherapeutics. Doxorubicin (DOX) is used as the model chemotherapeutic to evaluate the drug delivery efficacy of AmPDs in a drug-resistant breast cancer model. The AmPD/DOX nanoparticles would be able to improve the intracellular uptake and accumulation of DOX in breast cancer cell lines, particularly drug-resistant breast cancer cells, therefore exerting effective anticancer activity while circumventing drug-resistance.



Scheme 1. (A) Chemical structures of amphiphilic dendrimers (AmPDs). (B) Schematic illustration of the AmPDs mediated delivery of the anticancer drug doxorubicin (DOX). (The yellow parts of the amphiphilic peptide dendrimers represent the amine terminals of hydrophilic polylysine dendrons, and the blue parts represent the alkyl chain.

2. Materials and Methods

The full description of the materials and all the details of the related experiments are provided in the Supplementary Materials.

2.1. Materials

Doxorubicin hydrochloride was purchased from Beijing Fengtai Hualian Co. Ltd. (Beijing, China). Cell Counting Kit-8 (CCK-8), 3-(4,5-dimethylthiazol-2-yl)-2,5-diphenyltetrazolium bromide (MTT) was purchased from Sigma-Aldrich (Merck Life Science, Shanghai, China).

Human MCF-7 breast cancer cells (doxorubicin-sensitive cell line) were purchased from the Tongpai Biotechnology Co. Ltd. (Shanghai, China). Human MCF-7R breast cancer cells (doxorubicin-resistant cell line) were provided by Prof. Hulin Jiang (China Pharmaceutical University, Nanjing, China).

All other reagents were from Energy Chemical Ltd. (Shanghai, China), Sinopharm Chemical Reagent Co, Ltd. (Shanghai, China), Aladdin (Shanghai, China) or Sigma Aldrich (Shanghai, China) and used without any further purification.

2.2. Synthesis of AmPD KK₂

The synthetic protocol of hydrophobic alkyl chain and peptide dendrons was optimized (Supplementary Material) according to the reported literature [17,24,25]. AmPD 2-3, C₁₈-N₃, CuSO₄·5H₂O and NaAsc (L-Ascorbic Acid Sodium Salt) were dissolved in anhydrous THF under nitrogen atmosphere. Then the mixture was added to distilled water and stirred under nitrogen for 3 h at 50 °C. After solvent evaporation, the reaction mixture was extracted with CH₂Cl₂, washed with saturated NH₄Cl solution, brine, and then dried over Na₂SO₄. The residue was purified by silica gel column chromatography, yielding AmPD KK₂-Boc as white solid. Then AmPD KK₂-Boc was dissolved in anhydrous CH₂Cl₂, and trifluoroacetic acid (TFA) was added to the above solution under stirring at 0 °C. The mixture was stirred under nitrogen for 4 h at room temperature. After solvent evaporation, the residue was washed with anhydrous diethyl ether. The product was further purified by dialysis using a dialysis tube, followed by lyophilization to give AmPD KK₂ as white solid.

2.3. Synthesis of AmPD KK₂K₄

The synthetic protocol of AmPD KK₂K₄ was carried out similarly to the synthesis of AmPD KK₂, yielding a white solid.

All the detailed synthetic processes and characterization data of AmPDs were in the Supplementary Materials.

2.4. Critical Aggregation Concentration (CAC) of AmPDs Nanoassemblies

After sonicating for 5 min and resting at ambient temperature for 12 h, a fluorescence spectrophotometer was used to detect the AmPDs solution with Pyrene. The pyrene fluorescence spectra were recorded (an excitation wavelength: 334 nm).

2.5. Preparation of Doxorubicin-Loading Nanoformulations

The hydrophobic DOX was slowly added into the phosphate buffered saline (PBS) solution (0.01 M) containing AmPDs. The unencapsulated DOX was removed via a dialysis bag. The drug content loaded in the nanocarriers was calculated using the microplate reader (Cytation 5, BioTek, Winusky, VT, USA). The formulas of drug loading content and encapsulation efficiency are provided in the Supplementary Materials.

2.6. Size Distribution, and Zeta Potential Measurements

The size distribution of AmPDs nanoassemblies and AmPDs/DOX nanoformulations was determined by dynamic light scattering (DLS) using NanoBrookOmni (Brookhaven, Long Island, NY, USA). The final concentrations of AmPDs in both the AmPDs nanoassemblies solution and AmPDs/DOX nanoformulations solution was 2.0 mg/mL.

2.7. *In Vitro* Drug Release

AmPDs/DOX nanoformulations were dissolved in the buffer (pH 7.4 or 5.0) and transferred into dialysis bags. Then, these dialysis bags were immersed into a relevant buffer and kept in a shaking bed. At a series of sequential time points, the amounts of released doxorubicin were detected using a microplate reader. The cumulative amount of DOX released from nanoparticles was plotted against time.

2.8. Cell Culture

MCF-7 cells were maintained in DMEM (HyClone™-GE, Logan, UT, USA), with 10% Foundation™ Fetal Bovine Serum (FBS) (Gemini Bio-Products, Riverside Parkway, West Sacramento, CA, USA) added. MCF-7R cells were maintained in RMPI 1640 (HyClone™-GE, Logan, UT, USA), supplemented with 10% FBS. MCF-7 and MCF-7R cells were incubated at 37 °C with 5% CO₂.

2.9. *In Vitro* Anticancer Activity

The anticancer activities of AmPDs/DOX nanoformulations were performed on MCF-7 and MCF-7R cells. These cells were seeded and incubated at 37 °C for 24 h. After 24 h incubation, microculture tetrazolium solution was added and incubated. After removing the mediums, the cells were resuspended in dimethylsulfoxide (DMSO) solution. The absorbance of the DMSO solution was measured at 570 nm via a microplate reader. The cell metabolism toxicity and membrane damage toxicity of the blank carrier were also evaluated by MTT assay and lactate dehydrogenase (LDH) assay.

2.10. *In Vitro* Cellular Uptake

Flow cytometry: MCF-7R cells were seeded with a density of 6.0×10^4 cells per well and cultured. Then, the culture mediums were replaced with free DOX and AmPDs/DOX nanoformulations. After 30 min and 2 h incubation, cells were digested, washed, and resuspended with PBS solution, then analyzed using flow cytometry.

Confocal microscopy: MCF-7R cells were seeded into confocal dishes. After 4 h of incubation, mediums containing samples (AmDPs/DOX nanoformulations or free DOX) were introduced into the system. After the removal of mediums, cells were washed, and stained with lysotracker green and Hoechst 33,342. The cellular uptake of nanoformulations and free DOX were observed through two-photon confocal microscope (Zeiss, Oberkochen, Germany).

2.11. Drug Penetration in 3D-Cultured Tumor Spheroids

The MCF-7R 3D-cultured tumor spheroids were incubated with the free DOX or AmPDs/DOX nanoformulations. Four hours later, the medium containing the free DOX or AmPDs/DOX nanoformulations were removed and the tumor spheroids were washed and transferred to confocal dishes. The penetration of the 3D-cultured tumor spheroids at different depths was observed by a two-photon confocal microscope.

2.12. *In Vitro* Anticancer Activity in 3D-Cultured Tumor Spheroids

The MCF-7R 3D-cultured tumor spheroids were treated with culture mediums including AmPDs/DOX nanoformulations and free DOX at a serial of doxorubicin concentrations for 48 h. After adding the CCK-8 working solution into each well, the 3D-cultured tumor spheroids were incubated at 37 °C for 4 h. Then, the absorbance was measured via the microplate reader.

2.13. Statistical Tests

All data are presented as mean \pm SD unless otherwise indicated. Statistical analysis was performed by one-way ANOVA or two-way ANOVA with Tukey's post-hoc test (Graphpad Prism 8.01). * $p \leq 0.05$, ** $p \leq 0.01$, and *** $p \leq 0.001$.

3. Results and Discussion

3.1. Synthesis of the Amphiphilic Peptide Dendrimers (AmPDs)

AmPDs composed of hydrophobic C_{18} alkyl chain and different hydrophilic poly(L-lysine) peptide dendrons (AmPD KK_2 and AmPD KK_2K_4) were synthesized according to the strategy described in Schemes S1–S4 (Supplementary Materials). Different generations of Boc groups protected hydrophilic poly(L-lysine) dendrons bearing alkyne groups, and the hydrophobic C_{18} alkyl chains bearing an azide group were prepared using a previously reported protocol [17,24,25]. Then, hydrophilic dendrons were covalently conjugated with the hydrophobic alkyl chains via robust and efficient Cu(I)-catalyzed azide–alkyne cycloaddition (CuAAC) ‘click’ reaction to yield AmPDs with protecting groups. After the removal of their protecting groups (Boc groups), the terminal amines were exposed to obtain the AmPDs. The synthesis is described in further detail in the Supporting Information. The structures of these AmPDs were characterized using 1H NMR and mass spectrometry (Supplementary Materials).

3.2. Characterization of Self-Assembly Behaviours of AmPDs

Because of their amphiphilic nature, the AmPDs can self-assemble into nanoassemblies in an aqueous environment. The critical aggregation concentration (CAC) of AmPD KK_2K_4 ($14 \mu M$) was 2.3 times that of AmPD KK_2 ($6.1 \mu M$) (Figure 1A,B), indicating that AmPD KK_2 is more inclined to self-assemble into nanoassemblies than AmPD KK_2K_4 . This might be because AmPD KK_2 possesses a more favorable balance between its hydrophilic dendron and hydrophobic chain. Dynamic light scattering analysis revealed that the hydrodynamic sizes of the AmPD KK_2 and AmPD KK_2K_4 nanoassemblies were approximately 9.4 and 15 nm, respectively. Moreover, the zeta potential of AmPD KK_2 was 12.3 mV, which was slightly higher than that of AmPD KK_2K_4 (8.50 mV) (Figure 1C and Table S1). We also examined the secondary configurations of AmPD nanoassemblies using circular dichroism. The results shown in Figure 1D indicate that the AmPD KK_2 and AmPD KK_2K_4 nanoassemblies had similar secondary structures. These similarities were also confirmed by data analysis using CDNN software (Table S2). These results demonstrated that the AmPD nanoassemblies retain the inherent properties of polylysine.

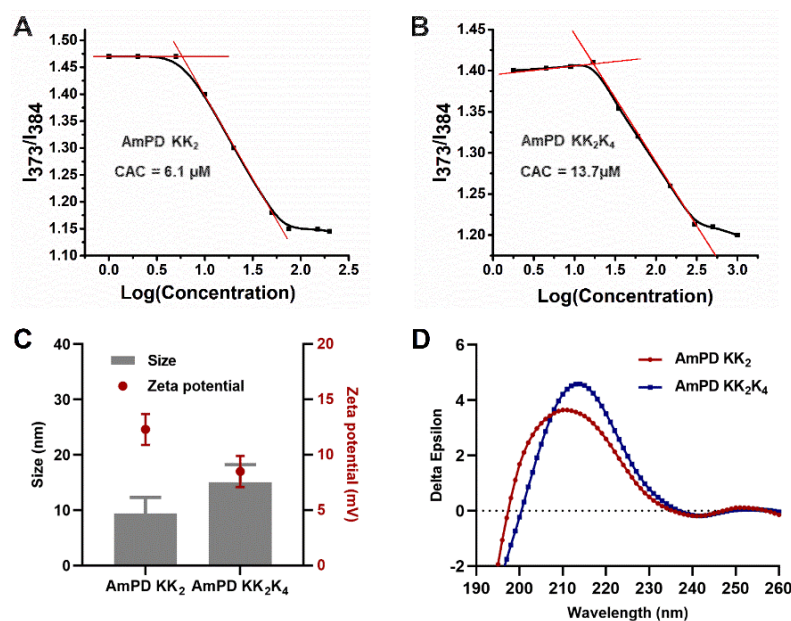


Figure 1. Physicochemical properties of the AmPDs. The CAC of the AmPD KK_2 (A) and AmPD KK_2K_4 (B) using the fluorescent dye pyrene. (C) Size and Zeta potential of the AmPDs nanoassemblies (mean \pm SD, $n = 3$). (D) The circular dichroism (CD) spectrum of the AmPDs nanoassemblies (0.50 mg/mL in H_2O).

3.3. Drug Encapsulation and Drug Release Profiles of DOX-Loaded AmPD Nanoformulations

DOX is a widely used, broad-spectrum anticancer drug that functions by intercalating into DNA to inhibit nucleic-acid synthesis. We selected DOX as a model drug to investigate drug encapsulation by the AmPD nanoassemblies. We used the film-dispersion method to prepare two DOX-loaded AmPD formulations: AmPD KK₂/DOX and AmPD KK₂K₄/DOX. These two formulations had a similar drug-loading content (~19%) and encapsulation efficiency (~97%) (Figure 2A). The size distribution of the AmPD KK₂/DOX and AmPD KK₂K₄/DOX formulations was approximately 73 and 80 nm, respectively (Figure 2B and Table S3). Their surface zeta potentials were 13.4 and 11.6 mV, respectively, indicating that they were in a stable colloidal state. These results demonstrated that the AmPD nanoassemblies could effectively package the hydrophobic anti-tumor drugs (DOX) via hydrophobic interaction to form stable DOX-loaded AmPDs nanoassemblies.

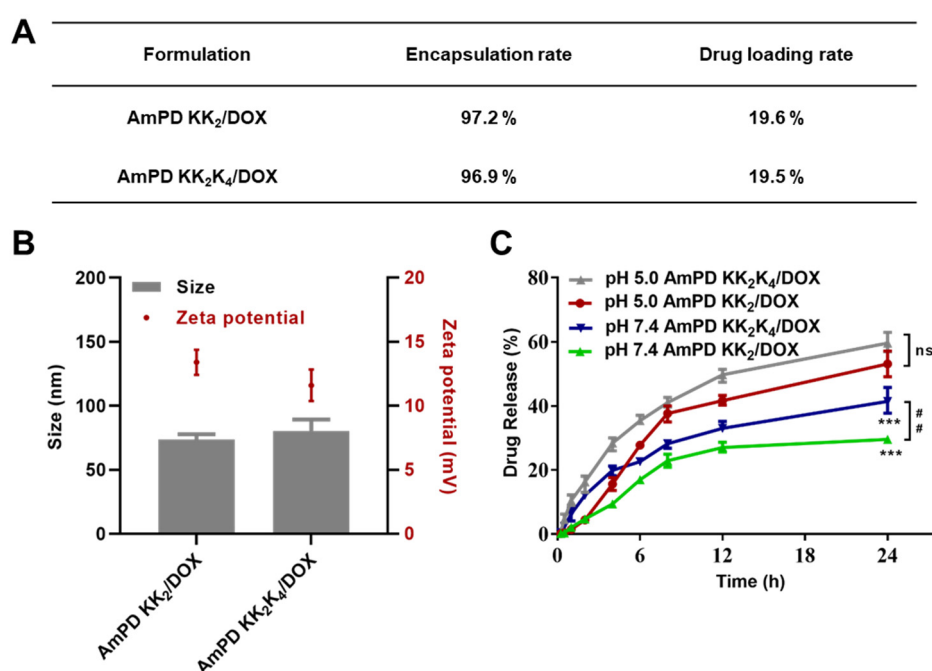


Figure 2. Physicochemical properties of the AmPDs/DOX nanoformulations. (A) Encapsulation efficiency and drug loading content of the AmPDs/DOX nanoformulations. (B) Size and Zeta potential of the AmPDs/DOX nanoformulations (mean \pm SD, $n = 3$). (C) The release of DOX from AmPDs/DOX nanoformulations at different pH values (5.0 and 7.4) (mean \pm SD, $n = 3$, ## $p < 0.01$ represented AmPD KK₂/DOX at pH 7.4 vs. AmPD KK₂K₄/DOX at pH 7.4, *** $p < 0.001$ represented AmPDs/DOX at pH 7.4 vs. AmPDs/DOX at pH 5.0, ns represented not statistically significant).

Controllable release of the loaded therapeutics at the tumor site is an important property of an effective drug delivery system. The acidity of the tumor microenvironment is lower than the normal tissue [26–28]. Thus, the ideal DDS should be able to reduce the release of the loaded drugs as little as possible under physiological conditions (pH 7.4) for safety consideration, while promoting drug release as much as possible under the acidic condition (pH 5.0) at the tumor site for therapeutic purposes. Hence, we evaluated the drug release profile of AmPDs/DOX nanoformulations at different pH values (5.0 and 7.4). The results showed that DOX was rapidly and efficiently released from the AmPDs/DOX nanoformulations at pH 5.0, with a cumulative release of more than 50% within 24 h (Figure 2C). The drug-release behavior of the AmPD KK₂-DOX and AmPD KK₂K₄-DOX nanoformulations was similar. We attribute this to the protonation of the encapsulated amine-bearing DOX at pH 5.0, resulting in electrostatic repulsion with positively charged amine-containing AmPD nanoassemblies, which promoted drug release under acidic conditions. However, in pH 7.4 buffer, the amount of drug released from AmPD KK₂/DOX

(about 25%) was substantially less than that from AmPD KK_2K_4 /DOX (about 41%). This difference is probably due to the better self-assembly capacity of AmPD KK_2 , which forms more stable formulations with hydrophobic drugs than AmPD KK_2K_4 , thereby providing better protection of the loaded cargo from leakage under physiological pH.

3.4. Potent Anticancer Efficacy of AmPD/DOX Nanoformulations via Effective Intracellular Uptake

After evaluating the drug-release characteristics of the AmPD/DOX nanoformulations, we evaluated their anticancer efficacy in human breast cancer cell lines, including DOX-sensitive MCF-7 cells and DOX resistant MCF-7R cells. First, we used MTT assays to examine their antiproliferative performance. In the DOX-sensitive MCF-7 cells, DOX-loaded AmPD nanoassemblies efficiently inhibited cell proliferation (Figure S1); the half-maximal inhibitory concentrations (IC_{50}) were 2.4 and 2.6 $\mu\text{g}/\text{mL}$ (or 4.4 and 4.9 μM) for AmPD KK_2 /DOX and AmPD KK_2K_4 /DOX, respectively; these values were similar to that of free DOX (Table S4). By contrast, in the DOX-resistant MCF-7R cells, AmPD/DOX had a much better anticancer effect with free DOX (Figure 3A and Figure S2). Interestingly, the IC_{50} of AmPD KK_2K_4 /DOX (7.0 $\mu\text{g}/\text{mL}$ or 47.8 μM) was approximately 2.7 times greater than that of AmPD KK_2 /DOX (26 $\mu\text{g}/\text{mL}$ or 12.9 μM) (Table S4), indicating that AmPD KK_2 /DOX induced a more potent antiproliferative effect than AmPD KK_2K_4 /DOX in MCF-7R cells.

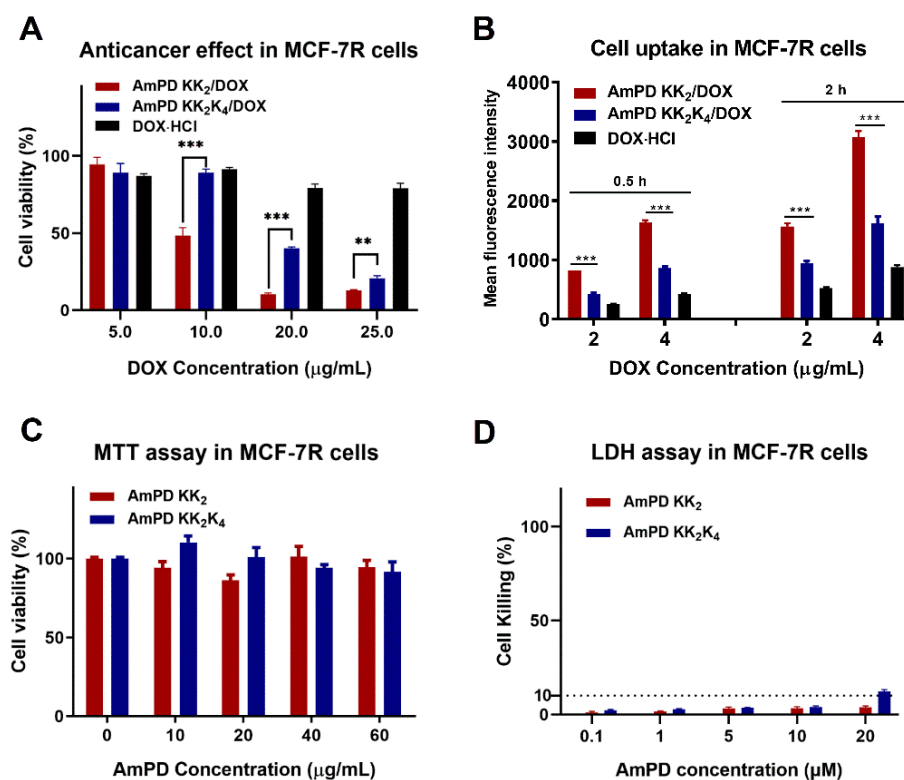


Figure 3. (A) The antiproliferative effect of AmPDs/DOX nanoformulations in MCF-7R cells by MTT assay (mean \pm SD, $n = 3$, ** $p < 0.01$, *** $p < 0.001$), (B) The cellular uptake of AmPDs/DOX nanoformulations in MCF-7R cells by flow cytometry analysis (mean \pm SD, $n = 3$, *** $p < 0.001$). The toxicity assessment of AmPD-based delivery systems in MCF-7R cells by MTT assay (C) and LDH assay (D) (mean \pm SD, $n = 3$).

We hypothesize that the different antiproliferative effects of the two AmPD/DOX nanoformulations in the drug-resistant cell line may be due to differences in their intracellular uptake. To validate this hypothesis, we carried out flow cytometry to quantify the intracellular uptake. As shown in Figure 3B, AmPDs/DOX nanoformulations facili-

tated efficient intracellular uptake of DOX in MCF-7R cells in a time- and dose-dependent manner. AmPD KK₂/DOX exhibited more effective cellular uptake of DOX than AmPD KK₂K₄/DOX at all times points and dosages. Such enhanced cellular uptake of AmPDs/DOX nanoformulations in MCF-7R cells was further confirmed by using confocal laser scanning microscopy (CLSM) (Figure S3). Moreover, after an additional 8 h of incubation, stronger fluorescent signals of DOX were detected for treatment with AmPD KK₂/DOX than with AmPD KK₂K₄/DOX (Figure S4), indicating more efficient intracellular accumulation of AmPD KK₂/DOX in MCF-7R cells.

We then assessed the safety profile of the AmPD delivery system in the two cell lines. As we expected, no notable metabolite toxicity was found even at a high concentration of AmPDs using MTT assays (Figure 3C and Figure S5), and no obvious damage to the cell membrane was detected by LDH assays (Figure 3D and Figure S6). This confirms the non-toxic characteristics of the AmPD delivery system.

Collectively, these results suggested that AmPD-based nanoassemblies can successfully deliver DOX into drug-resistant MCF-7R cancer cells, enhance the intracellular retention of DOX, and thereby induce a potent anticancer effect. Interestingly, AmPD KK₂ facilitated more efficient intracellular uptake and retention of DOX than AmPD KK₂K₄, thereby more effectively inhibiting cell proliferation.

3.5. Deep Drug Penetration and Cellular Uptake in 3D-Cultured Tumor Spheroids

3D tumor spheroids can retain the material and structural basis of the tumor microenvironment, rendering them an attractive in vitro model that mimics the real tumor environment [29,30]. Thus, we used employed 3D-cultured tumor spheroids to study the drug delivery mediated by AmPDs. First, we utilized CLSM measurements to trace the penetration and uptake behavior of the AmPDs/DOX nanoformulations in MCF-7R tumor spheroids. Strong fluorescent signals of DOX were observed for treatments with the AmPDs/DOX nanoformulations, whereas very weak signals were observed upon treatment with free DOX (Figure 4A,B). These results unambiguously confirm that, in contrast with free DOX, the AmPDs/DOX nanoformulations penetrated deep into the interior of the tumor spheroids.

We further measured the cellular uptake of the AmPDs/DOX nanoformulations in MCF-7R cells inside the tumor spheroids using flow cytometry. As illustrated in Figure 4C, AmPDs/DOX nanoformulations substantially enhanced the uptake and accumulation of DOX in MCF-7R cells of the tumor spheroids, which corroborates the results of the CLSM measurements. Similar to the situation in the 2D model, AmPD KK₂/DOX exhibited better penetration behavior than AmPD KK₂K₄/DOX in the 3D tumor spheroids. This difference in performance might be due to the more stable AmPD KK₂/DOX formulation better protecting the DOX from leakage before penetrating into the interior of the tumor spheroid. This would result in more efficient penetration and cellular uptake of DOX in the tumor cells inside the spheroids.

3.6. Enhanced Antiproliferative Effect in 3D-Cultured Tumor Spheroids

Encouraged by the enhanced penetration and cellular internalization of the AmPDs/DOX nanoformulations in the tumor spheroids, we further evaluated their antiproliferative effect. The results shown in Figure 4D suggest that the AmPDs/DOX nanoformulations induce a potent, dose-dependent antiproliferative effect, in contrast with free DOX, which did not inhibit cell proliferation. Specifically, the IC₅₀ of AmPD KK₂/DOX (48.4 µg/mL or 89.1 µM) was approximately 3.5 times lower than AmPD KK₂K₄/DOX (138.5 µg/mL or 254.8 µM) (Table S4), showing that proliferation was much more efficiently inhibited by treatment with AmPD KK₂/DOX. We attribute this enhanced antiproliferative effect to the more efficient penetration and internalization of AmPD KK₂/DOX in the tumor spheroids. These results demonstrate that although both AmPDs/DOX nanoformulations can effectively inhibit the proliferation of 3D tumor spheroids, AmPD KK₂/DOX is the better potential candidate for cancer therapy.

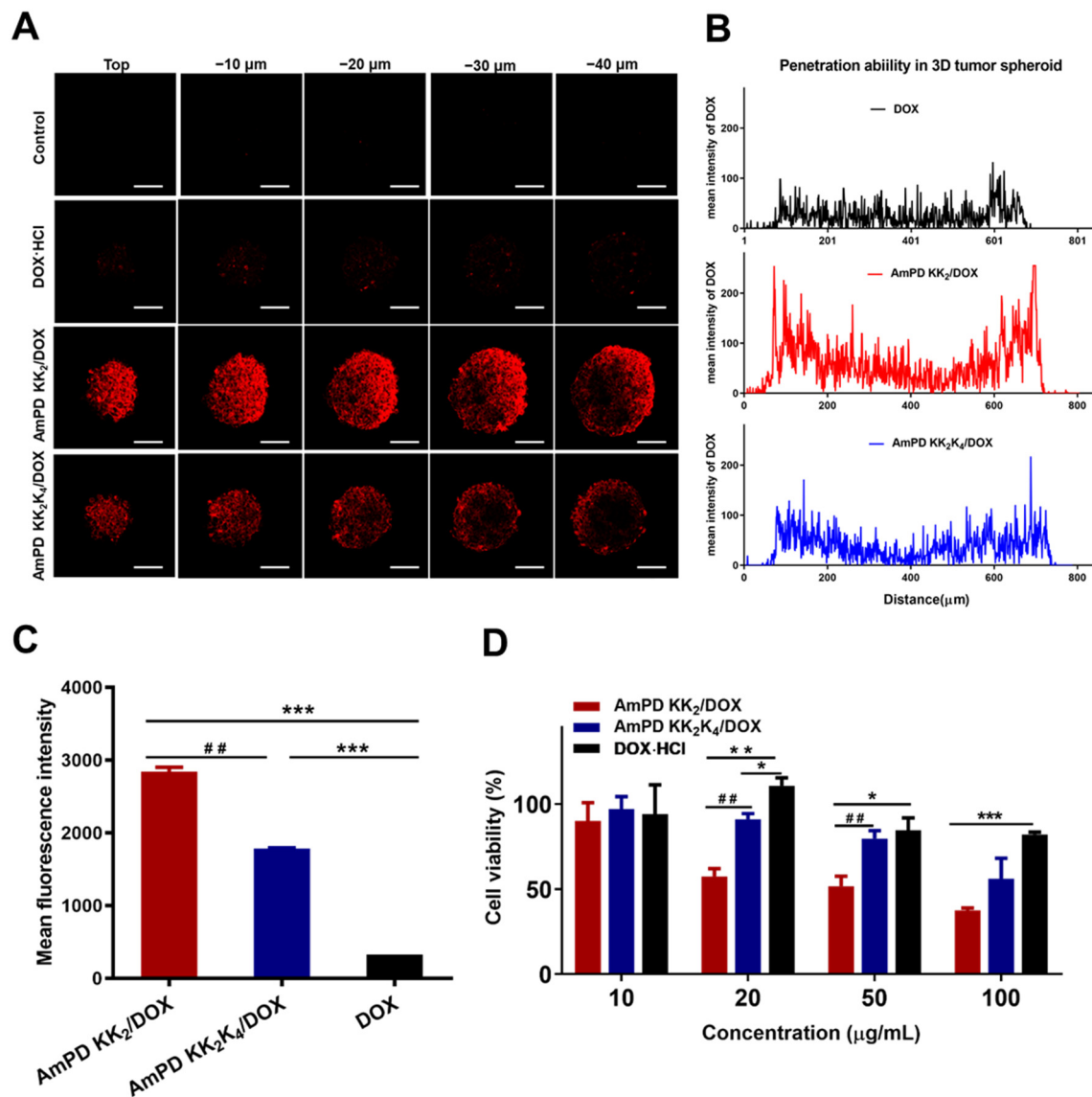


Figure 4. Penetration and anticancer activity of AmPDs/DOX nanoformulations in MCF-7R 3D-cultured tumor spheroids. (A) Confocal microscopic imaging of the penetration of AmPDs/DOX in tumor spheroids. The red channel image shows DOX (Scale bars, 100 μm). (B) Line-scanning profiles of fluorescence intensity of tumor spheroids after treating with free DOX, AmPD KK₂/DOX and AmPD KK₂K₄/DOX. (C) Flow cytometry analysis of the cellular uptake in tumor spheroids after incubating with free DOX, AmPD KK₂/DOX and AmPD KK₂K₄/DOX (mean \pm SD, $n = 3$, ## $p < 0.01$ represented AmPD KK₂/DOX vs. AmPD KK₂K₄/DOX, *** $p < 0.001$ represented AmPDs/DOX vs. DOX). (D) The anticancer activity evaluation by CCK-8 assays after the treatment with free DOX, AmPD KK₂/DOX and AmPD KK₂K₄/DOX in tumor spheroids (mean \pm SD, $n = 3$, ## $p < 0.01$ represented AmPD KK₂/DOX vs. AmPD KK₂K₄/DOX, * $p < 0.05$, ** $p < 0.01$ and *** $p < 0.001$ represented AmPDs/DOX vs. DOX).

4. Conclusions

Despite being a mainstay in clinical treatment, chemotherapy is limited by its severe side effects and inherent or acquired drug resistance. Nanotechnology-based drug-delivery systems are widely expected to improve therapeutic efficacy while reducing toxicity for anticancer treatment. In this study, we developed a novel self-assembling drug-delivery system based on amphiphilic peptide dendrimers (AmPDs) bearing a hydrophobic C₁₈ chain and a hydrophilic peptide dendron with different generations (AmPD KK₂ and AmPD KK₂K₄). The AmPDs self-assembled into nanoassemblies and effectively encapsulate the antitumor drug (DOX) to form stable nanoformulations (AmPD KK₂/DOX and

AmPD KK₂K₄/DOX). The AmPD/DOX nanoformulations conquered drug resistance in drug-resistant breast cancer MCF-7R cells owing to their enhanced intracellular uptake and accumulation of DOX, and in 3D-cultured tumor spheroids owing to their efficient penetration. Thus, a potent anticancer effect was achieved in 2D and 3D breast cancer models. Interestingly, AmPD KK₂, which had a smaller peptide dendron than AmPD KK₂K₄, can encapsulate DOX to form more stable nanoparticles, resulting in better cellular uptake, penetration, and anti-proliferative activity. This may be because AmPD KK₂ maintains a better balance between hydrophobic and hydrophilic entities. Collectively, this work provides a promising new perspective on the design of safe and efficient drug-delivery platforms for cancer therapy based on self-assembling amphiphilic peptide dendrimers.

Supplementary Materials: The following are available online at <https://www.mdpi.com/article/10.3390/pharmaceutics13071092/s1>, Scheme S1. Synthesis and conditions of hydrophobic alkyl chain, Scheme S2. Synthesis and conditions of AmPDs, Scheme S3. Synthetic route of the AmPD KK₂, Scheme S4. Synthetic route of the AmPD KK₂K₄, Figure S1. The antiproliferative effect of the AmPDs/DOX nanoformulations in MCF-7 cells by MTT assay, Figure S2. The antiproliferative effect of the AmPDs/DOX nanoformulations in MCF-7R cells by MTT assay, Figure S3. Confocal microscopic imaging of the cellular uptake of the AmPDs/DOX nanoformulations in MCF-7R cells, Figure S4. The intracellular accumulation of AmPDs/DOX nanoformulations in MCF-7R cells by flow cytometry analysis, Figure S5. Metabolic toxicity of the AmPDs nanoassemblies in MCF-7 cells by MTT assay, Figure S6. Membrane injury toxicity of the AmPDs nanoassemblies in MCF-7 cells by LDH assay, Table S1. Size and Zeta potential of the AmPDs nanoassemblies, Table S2. Data analysis of CD spectrum of AmPDs nanoassemblies by CDNN software, Table S3. Size and Zeta potential of the AmPDs/DOX nanoformulations, Table S4. The half-maximal inhibitory concentrations (IC₅₀) of AmPDs/DOX nanoformulations in MCF-7 cells, MCF-7R cells and MCF-7R 3D-cultured tumor spheroids.

Author Contributions: Conceptualization, N.L., W.Z. and X.L.; Project administration, N.L., W.Z. and X.L.; Formal analysis, D.Z., H.Z., B.L., C.M., Y.C. and S.W.; Funding acquisition, N.L. and X.L.; Investigation, D.Z., H.Z., Y.H. and L.H.; Methodology, D.Z., H.Z., Y.H., B.L., C.M., N.L. and W.Z.; Supervision, X.L.; Writing—original draft, D.Z., H.Z., N.L. and X.L.; Writing—review & editing, D.Z., H.Z., Y.H., B.L., C.M., L.H., Y.C., S.W., N.L., W.Z. and X.L. All authors have read and agreed to the published version of the manuscript.

Funding: This work was financially supported by National Key Research & Development Program of China for International S&T Cooperation Projects (2018YFE0117800), the National Natural Science Foundation of China (No. 51773227, 81701815, 51703245), Natural Science Foundation of Jiangsu Province (BK20170735, BK20170733), the Youth Thousand-Talents Program of China, the Program for Jiangsu Province Innovative Research Talents, the Program for Jiangsu Province Innovative Research Team, the Six Talent Peaks Project in Jiangsu Province of China, the Jiangsu Specially-Appointed Professors Program, the State Key Laboratory of Natural Medicines at China Pharmaceutical University (No. SKLNMZZ202007), “Double First-Class” project of China Pharmaceutical University (CPU2018GF05) and the Open Project of Key Laboratory of Biomedical Engineering of Guangdong Province (KLBEMGD201802).

Institutional Review Board Statement: Not applicable.

Informed Consent Statement: Not applicable.

Data Availability Statement: Not applicable.

Conflicts of Interest: The authors declare no conflict of interest.

References

1. Bray, F.; Ferlay, J.; Soerjomataram, I.; Siegel, R.L.; Torre, L.A.; Jemal, A. Global cancer statistics 2018: GLOBOCAN estimates of incidence and mortality worldwide for 36 cancers in 185 countries. *CA Cancer J. Clin.* **2018**, *68*, 394–424. [CrossRef]
2. Hulvat, M.C. Cancer Incidence and Trends. *Surg. Clin. N. Am.* **2020**, *100*, 469–481. [CrossRef]
3. Vasan, N.; Baselga, J.; Hyman, D.M. A view on drug resistance in cancer. *Nature* **2019**, *575*, 299–309. [CrossRef]
4. Shibue, T.; Weinberg, R.A. EMT, CSCs, and drug resistance: The mechanistic link and clinical implications. *Nat. Rev. Clin. Oncol.* **2017**, *14*, 611–629. [CrossRef]

5. Alfarouk, K.O.; Stock, C.-M.; Taylor, S.; Walsh, M.; Muddathir, A.K.; Verduzco, D.; Bashir, A.H.H.; Mohammed, O.Y.; ElHassan, G.O.; Harguindey, S.; et al. Resistance to cancer chemotherapy: Failure in drug response from ADME to P-gp. *Cancer Cell Int.* **2015**, *15*, 71. [[CrossRef](#)]
6. Bourzac, K. Nanotechnology carrying drugs. *Nature* **2012**, *491*, 58–60. [[CrossRef](#)]
7. Shi, J.; Kantoff, P.W.; Wooster, R.; Farokhzad, J.S.O.C. Cancer nanomedicine: Progress, challenges and opportunities. *Nat. Rev. Cancer* **2017**, *17*, 20–37. [[CrossRef](#)]
8. Minko, T. Nanotechnology and drug resistance preface. *Adv. Drug Deliv. Rev.* **2013**, *65*, 1665–1666. [[CrossRef](#)]
9. Ward, R.A.; Fawell, S.; Floc'H, N.; Flemington, V.; McKerrecher, D.; Smith, P.D. Challenges and Opportunities in Cancer Drug Resistance. *Chem. Rev.* **2021**, *121*, 3297–3351. [[CrossRef](#)]
10. Fang, J.; Nakamura, H.; Maeda, H. The EPR effect: Unique features of tumor blood vessels for drug delivery, factors involved, and limitations and augmentation of the effect. *Adv. Drug Deliv. Rev.* **2011**, *63*, 136–151. [[CrossRef](#)]
11. Gao, Z.; Zhang, L.; Sun, Y. Nanotechnology applied to overcome tumor drug resistance. *J. Control. Release* **2012**, *162*, 45–55. [[CrossRef](#)]
12. Wei, T.; Chen, C.; Liu, J.; Liu, C.; Posocco, P.; Liu, X.; Cheng, Q.; Huo, S.; Liang, Z.; Fermeglia, M.; et al. Anticancer drug nanomicelles formed by self-assembling amphiphilic dendrimer to combat cancer drug resistance. *Proc. Natl. Acad. Sci. USA* **2015**, *112*, 2978–2983. [[CrossRef](#)]
13. Petros, R.A.; DeSimone, J.M. Strategies in the design of nanoparticles for therapeutic applications. *Nat. Rev. Drug Discov.* **2010**, *9*, 615–627. [[CrossRef](#)] [[PubMed](#)]
14. Svenson, S.; Tomalia, D.A. Dendrimers in biomedical applications—Reflections on the field. *Adv. Drug Deliv. Rev.* **2005**, *57*, 2106–2129. [[CrossRef](#)] [[PubMed](#)]
15. Lee, C.C.; Mackay, J.A.; Frechet, J.; Szoka, F.C. Designing dendrimers for biological applications. *Nat. Biotechnol.* **2005**, *23*, 1517–1526. [[CrossRef](#)]
16. Lyu, Z.; Ding, L.; Tintaru, A.; Peng, L. Self-Assembling Supramolecular Dendrimers for Biomedical Applications: Lessons Learned from Poly(amidoamine) Dendrimers. *Acc. Chem. Res.* **2020**, *53*, 2936–2949. [[CrossRef](#)]
17. Yu, T.; Liu, X.; Bolcato-Bellemin, A.-L.; Wang, Y.; Liu, C.; Erbacher, P.; Qu, F.; Rocchi, P.; Behr, J.-P.; Peng, L. An Amphiphilic Dendrimer for Effective Delivery of Small Interfering RNA and Gene Silencing In Vitro and In Vivo. *Angew. Chem. Int. Ed.* **2012**, *51*, 8478–8484. [[CrossRef](#)] [[PubMed](#)]
18. Liu, X.; Zhou, J.; Yu, T.; Chen, C.; Cheng, Q.; Sengupta, K.; Huang, Y.; Li, H.; Liu, C.; Wang, Y.; et al. Adaptive amphiphilic dendrimer-based nanoassemblies as robust and versatile siRNA delivery systems. *Angew. Chem. Int. Ed.* **2014**, *53*, 11822–11827. [[CrossRef](#)]
19. Liu, X.; Wang, Y.; Chen, C.; Tintaru, A.; Cao, Y.; Liu, J.; Ziarelli, F.; Tang, J.; Guo, H.; Rosas, R.; et al. A Fluorinated Bola-Amphiphilic Dendrimer for On-Demand Delivery of siRNA, via Specific Response to Reactive Oxygen Species. *Adv. Funct. Mater.* **2016**, *26*, 8594–8603. [[CrossRef](#)]
20. Dong, Y.; Yu, T.; Ding, L.; Laurini, E.; Huang, Y.; Zhang, M.; Weng, Y.; Lin, S.; Chen, P.; Marson, D.; et al. A dual targeting dendrimer-mediated siRNA delivery system for effective gene silencing in cancer therapy. *J. Am. Chem. Soc.* **2018**, *140*, 16264–16274. [[CrossRef](#)]
21. Sapra, R.; Verma, R.P.; Maurya, G.P.; Dhawan, S.; Babu, J.; Haridas, V. Designer Peptide and Protein Dendrimers: A Cross-Sectional Analysis. *Chem. Rev.* **2019**, *119*, 11391–11441. [[CrossRef](#)]
22. Zhang, X.; Xu, X.; Li, Y.; Hu, C.; Zhang, Z.; Gu, Z. Virion-Like Membrane-Breaking Nanoparticles with Tumor-Activated Cell-and-Tissue Dual-Penetration Conquer Impermeable Cancer. *Adv. Mater.* **2018**, *30*, e1707240. [[CrossRef](#)]
23. Dong, Y.; Chen, Y.; Zhu, D.; Shi, K.; Ma, C.; Zhang, W.; Rocchi, P.; Jiang, L.; Liu, X. Self-assembly of amphiphilic phospholipid peptide dendrimer-based nanovectors for effective delivery of siRNA therapeutics in prostate cancer therapy. *J. Control. Release* **2020**, *322*, 416–425. [[CrossRef](#)]
24. Ma, C.; Zhu, D.; Chen, Y.; Dong, Y.; Lin, W.; Li, N.; Zhang, W.; Liu, X. Amphiphilic peptide dendrimer-based nanovehicles for safe and effective siRNA delivery. *Biophys. Rep.* **2020**, *6*, 278–289. [[CrossRef](#)]
25. Luo, K.; Li, C.; Li, L.; She, W.; Wang, G.; Gu, Z. Arginine functionalized peptide dendrimers as potential gene delivery vehicles. *Biomaterials* **2012**, *33*, 4917–4927. [[CrossRef](#)]
26. Tannock, I.F.; Rotin, D. Acid pH in tumors and its potential for therapeutic exploitation. *Cancer Res.* **1989**, *49*, 4373–4384.
27. Gatenby, R.A.; Gillies, R. Why do cancers have high aerobic glycolysis? *Nat. Rev. Cancer* **2004**, *4*, 891–899. [[CrossRef](#)]
28. Webb, B.A.; Chimenti, M.; Jacobson, M.P.; Barber, D.L. Dysregulated pH: A perfect storm for cancer progression. *Nat. Rev. Cancer* **2011**, *11*, 671–677. [[CrossRef](#)] [[PubMed](#)]
29. Nath, S.; Devi, G.R. Three-dimensional culture systems in cancer research: Focus on tumor spheroid model. *Pharmacol. Ther.* **2016**, *163*, 94–108. [[CrossRef](#)] [[PubMed](#)]
30. Ishiguro, T.; Ohata, H.; Sato, A.; Yamawaki, K.; Enomoto, T.; Okamoto, K. Tumor-derived spheroids: Relevance to cancer stem cells and clinical applications. *Cancer Sci.* **2017**, *108*, 283–289. [[CrossRef](#)] [[PubMed](#)]